Energy Advances

ROYAL SOCIETY OF CHEMISTRY

PAPER

View Article Online
View Journal

Cite this: DOI: 10.1039/d6ya00031b

Enhancing light and dark photocatalytic hydrogen production *via* graphene conductive networks in carbon nitride composites

Zejun Zhang,[a] Fankai Bu,[a] Songmei Wang,[a] Zhidong Wei,[c] Yong Zhu*[b] and Junying Liu *[a]

The development of photocatalysts capable of operating under both light and dark conditions is critical for sustainable solar energy utilization. This study presents a graphene-enhanced cyano-functionalized carbon nitride composite, fabricated *via* a simple electrostatic assembly method, to achieve efficient photocatalytic hydrogen evolution during day–night cycles. The introduction of graphene does not alter the structure of ^{NCN}CN. Graphene functions as an electron-conductive network, significantly improving charge separation and storage capabilities. Under visible light ($\lambda \geq 400$ nm), the optimal composite with 0.5 wt% graphene exhibited a hydrogen production rate of 3156 μmol h^{-1} g^{-1}, 35% higher than that of pure ^{NCN}CN. Remarkably, under dark conditions, it achieved a hydrogen yield of 3.8 μmol, representing a 65% enhancement. Photoelectrochemical analyses validated the reduced recombination of electron–hole pairs and enhanced conductivity. The proposed mechanism highlights the role of graphene in facilitating electron transfer to Pt co-catalysts and storing electrons *via* cyanide-K^+ pairs for delayed hydrogen production in the dark. This work demonstrates the potential of graphene-based composites as efficient all-weather photocatalysts for sustainable energy applications.

Received 11th February 2026,
Accepted 23rd March 2026

DOI: 10.1039/d6ya00031b

rsc.li/energy-advances

1. Introduction

With rapid economic development, fossil fuels are being heavily utilized, leading to a significant increase in greenhouse gas emissions.[1] Therefore, the development of sustainable clean energy is imperative. Solar energy, as one of the most important sustainable clean energy sources, has attracted considerable attention since the 1970s.[2] Recently, H_2 production *via* solar-driven photocatalytic water splitting on semiconductor materials has been extensively studied as an attractive pathway.[3] However, the poor solar-to-hydrogen conversion efficiency of semiconductor photocatalysts severely limits the practical development of photocatalytic water splitting, due to their inefficient charge separation/transfer, limited light absorption capacity, and poor surface reactions.[4,5] To address these challenges, developing high-performance photocatalysts is necessary. In this context, carbon nitride has garnered widespread attention due to its excellent physical properties and tunable composition/morphology/chemical structure.[6,7] It possesses a favorable electronic structure with a band gap of 2.7 eV.[8] Additionally, it offers the advantages of being easily obtainable at low cost, high stability, and a tunable structure.[9,10] Although carbon nitride suffers from drawbacks such as high recombination rates of photogenerated electron–hole pairs, its photocatalytic performance can be improved through methods like morphology modification,[11] doping,[12–14] co-catalyst modification,[15] and constructing composite heterojunctions.[16–18]

Furthermore, some researchers have combined carbon nitride with graphene to improve its conductivity and catalytic performance. Graphene, a two-dimensional macromolecular sheet of carbon atoms with a honeycomb structure, has attracted significant attention due to its outstanding mechanical, thermal, optical, and electrical properties, as well as its wide application in nanoelectronics, biosensing, polymer composites, capacitors, and catalysts.[19,20] Moreover, graphene's high thermal conductivity ensures excellent charge carrier mobility. Graphene can be easily produced from natural graphite at a low cost through chemical oxidation, dispersion, and reduction processes. Indeed, due to its excellent properties and high compatibility, there are numerous examples of graphene applications in photocatalysis. For instance, Zhang *et al.*[21] reported a nano-TiO_2 (P25)-graphene composite photocatalyst for the photocatalytic degradation of methylene blue. Mietek Jaroniec *et al.*[22] prepared a graphene/g-C_3N_4 composite for

[a] School of Environment and Safety Engineering, Jiangsu University, 301 Xuefu Road, Zhenjiang 212013, China. E-mail: lsliujy@ujs.edu.cn
[b] College of Mechanical and Power Engineering, East China University of Science and Technology, Shanghai 200237, China. E-mail: zyong@ecust.edu.cn
[c] College of Smart Energy, Shanghai Jiao Tong University, Shanghai 200030, China

photocatalytic water splitting to produce hydrogen. Huaming Li *et al.*[23] fabricated an mpg-C_3N_4 composite modified with hydroxyl graphene quantum dots.

Although numerous studies have sought to enhance the photocatalytic hydrogen production performance of g-C_3N_4, a key limitation remains its lack of activity in dark environments. Particularly, recently, some researchers have focused on photocatalysis under dark conditions.[24] Lotsch *et al.*[25] reported a cyanamide-functionalized carbon nitride based on heptazine units. This carbon nitride forms highly reductive radicals in the presence of an electron donor under sunlight irradiation, with lifetimes extending beyond day–night cycles. These radical species form within the cyanamide-functionalized polymer network of the heptazine units and can release their trapped electrons in the dark to produce H_2, triggered by a co-catalyst. Other studies have also involved dark catalysis of carbon nitride, but these primarily focus on modifying and optimizing carbon nitride itself, with few other related reports.

In this study, we report a strategy for preparing G–^{NCN}CN composite photocatalysts *via* static electrical assembly of cyanamide-functionalized carbon nitride and graphene. The effect of different graphene contents on the photocatalytic hydrogen production efficiency from an aqueous triethanolamine solution under visible light irradiation was discussed. The morphology, structure, and photoelectrochemical properties of the G–^{NCN}CN composite were characterized using various physicochemical methods. The results indicate that the introduction of graphene significantly enhances the catalytic performance of the G–^{NCN}CN composite compared to that of pure ^{NCN}CN. Meanwhile, graphene serves as a conductive network, significantly enhancing the electron storage capacity of the G–^{NCN}CN composite and strengthening its ability for hydrogen production from water splitting under dark conditions.

2. Experimental

2.1. Chemicals and reagents

Graphene, chloroplatinic acid, triethanolamine, and 4-MBA were provided by Shanghai Aladdin Biochemical Technology Co., Ltd. Melamine (≥99%) and potassium thiocyanate (≥99%) were provided by Shanghai Macklin Biochemical Technology Co., Ltd. All chemicals were used as received without further purification.

2.2. Synthesis of cyano-containing carbon nitride

Cyanamide-functionalized carbon nitride (^{NCN}CN) was synthesized *via* a two-step thermal process.[26] In the first step, bulk graphitic carbon nitride (bulk g-C_3N_4) was prepared by heating 10 g of melamine in a covered alumina crucible within a muffle furnace. The temperature was raised to 550 °C at a rate of 3 °C min^{-1} and maintained for 3 h, followed by natural cooling to room temperature to obtain a yellow CN powder. Subsequently, 500 mg of the as-prepared melamine was thoroughly mixed with 1 g of potassium thiocyanate (KSCN). The finely ground mixture was placed in a covered ceramic boat and heated under a nitrogen atmosphere. The temperature was first increased to 400 °C at 3 °C min^{-1}, held for 1 h, and then rapidly raised to 550 °C for an additional 30 min. After cooling, the resulting product was washed with deionized water, collected by centrifugation, and dried, yielding a yellow powder identified as ^{NCN}CN.

2.3. Synthesis of the G–^{NCN}CN composite

The G–^{NCN}CN composite was synthesized *via* a straightforward electrostatic assembly approach. Briefly, 10 mg of the as-prepared ^{NCN}CN photocatalyst was dispersed in 80 mL of deionized water. Subsequently, a graphene solution, equivalent to 0.5 wt% of the ^{NCN}CN mass, was introduced into the mixture. The suspension was magnetically stirred continuously for 10 h to facilitate the integration of ^{NCN}CN with graphene, yielding the final composite material.

2.4. Characterization

The crystal structures of the samples were analyzed by powder X-ray diffraction (XRD) on a Bruker D8 ADVANCE diffractometer. Morphological and microstructural analyses were carried out using transmission electron microscopy (TEM) on an HT-7800 microscope and a TF20 high-resolution transmission electron microscope (HRTEM) operating at 120 kV and 200 kV, respectively. The surface chemical states were investigated by X-ray photoelectron spectroscopy (XPS) using an ESCALAB QXi spectrometer with a monochromatic Al Kα X-ray source. Fourier transform infrared (FTIR) spectra were recorded on a Thermo Fisher Nicolet Is5 spectrometer. UV-Visible absorption spectra were obtained using a Shimadzu UV-2600 spectrophotometer. Photoluminescence (PL) spectra and transient fluorescence decay curves were measured at room temperature on a Gangdong Science and Technology F-320 spectrophotometer and an Edinburgh FLS 1000 fluorescence spectrophotometer, respectively. The photoelectrochemical properties, including the photocurrent response and electrochemical impedance spectroscopy (EIS), were evaluated using a CHI-660F electrochemical workstation.

2.5. Photocatalytic hydrogen production

Photocatalytic H_2 production reactions under visible light were carried out by dispersing 10 mg of the prepared material into 80 mL of an aqueous solution containing 4 mL of triethanolamine. The photocatalytic water splitting reaction was performed in an irradiation reaction vessel connected to a glass-enclosed gas system. Prior to the hydrogen evolution reaction, in a typical procedure, 10 mg of Pt-loaded catalyst was dispersed into 80 mL of an aqueous solution containing 4 mL of triethanolamine. The system was evacuated several times to completely remove residual air. The evolved gases were analyzed using gas chromatography (GC-7920) equipped with a TCD detector, using argon as the carrier gas. Visible light was provided by a 300 W xenon lamp using a filter ($\lambda \geq 400$ nm). The temperature of the reaction system was maintained at 15 °C using a cooling water flow.

3. Results and discussion

The structural characteristics of the G–^{NCN}CN samples were analyzed using XRD. As shown in Fig. 1a, all samples, including the composite with 0.5 wt% graphene loading (0.5 wt% G–^{NCN}CN), exhibit similar diffraction patterns. This indicates that the fundamental structure of the ^{NCN}CN matrix is preserved after graphene incorporation. CN exhibits two distinct diffraction peaks at 12.9° and 27.2°. The distinct peaks at approximately 27.2° in the pure CN sample correspond to the (002) interplanar stacking of graphitic carbon nitride.[26] In contrast, this peak shifts to a higher angle of 28.2° in both the pure ^{NCN}CN and the 0.5 wt% G–^{NCN}CN composite, corresponding to a smaller interlayer spacing. This shift suggests a denser interlayer packing in the ^{NCN}CN-based materials. Due to the ability of molten salt to enhance the crystallinity of carbon nitride, the (100) diffraction peak at 12.9° shifts toward smaller angles compared to the diffraction peak of CN. Although a characteristic (002) peak of graphene is observed at 26.2° in the pure graphene sample, this peak is absent in the XRD pattern of the composite due to the low concentration and high dispersion of graphene, which is below the detection limit of XRD.[27]

Furthermore, the chemical structures of pristine CN, ^{NCN}CN and 0.5 wt% G–^{NCN}CN were examined by FT-IR spectroscopy, as shown in Fig. 1b. The spectra of all three samples exhibit strong similarity in the region of 800–1650 cm^{-1}. The characteristic peaks of the heptazine core at approximately 804 cm^{-1} and the bridging C–N bending vibrations at 1208 and 1307 cm^{-1} are preserved in both ^{NCN}CN and the 0.5 wt% G–^{NCN}CN composite, indicating that the fundamental structure of the carbon nitride matrix remains intact after modification. The key difference for the ^{NCN}CN-based samples is the appearance of a distinct peak at 2181 cm^{-1}, which is attributed to the C≡N stretching vibration of surface cyanamide groups.[28,29] Furthermore, the 0.5 wt% G–^{NCN}CN composite exhibits a new peak at 1564 cm^{-1}, corresponding to the skeletal vibration of graphene sheets.[30] This confirms the successful incorporation of graphene into the composite without altering the primary structure of the ^{NCN}CN host.

The optical properties of pristine CN, ^{NCN}CN and 0.5 wt% G–^{NCN}CN were characterized by UV-Vis diffuse reflectance spectroscopy, as shown in Fig. 1c. Since the liquid concentration is not high, graphene exhibits a relatively low and featureless absorption across the 400–800 nm visible light range, while ^{NCN}CN demonstrates significantly enhanced light

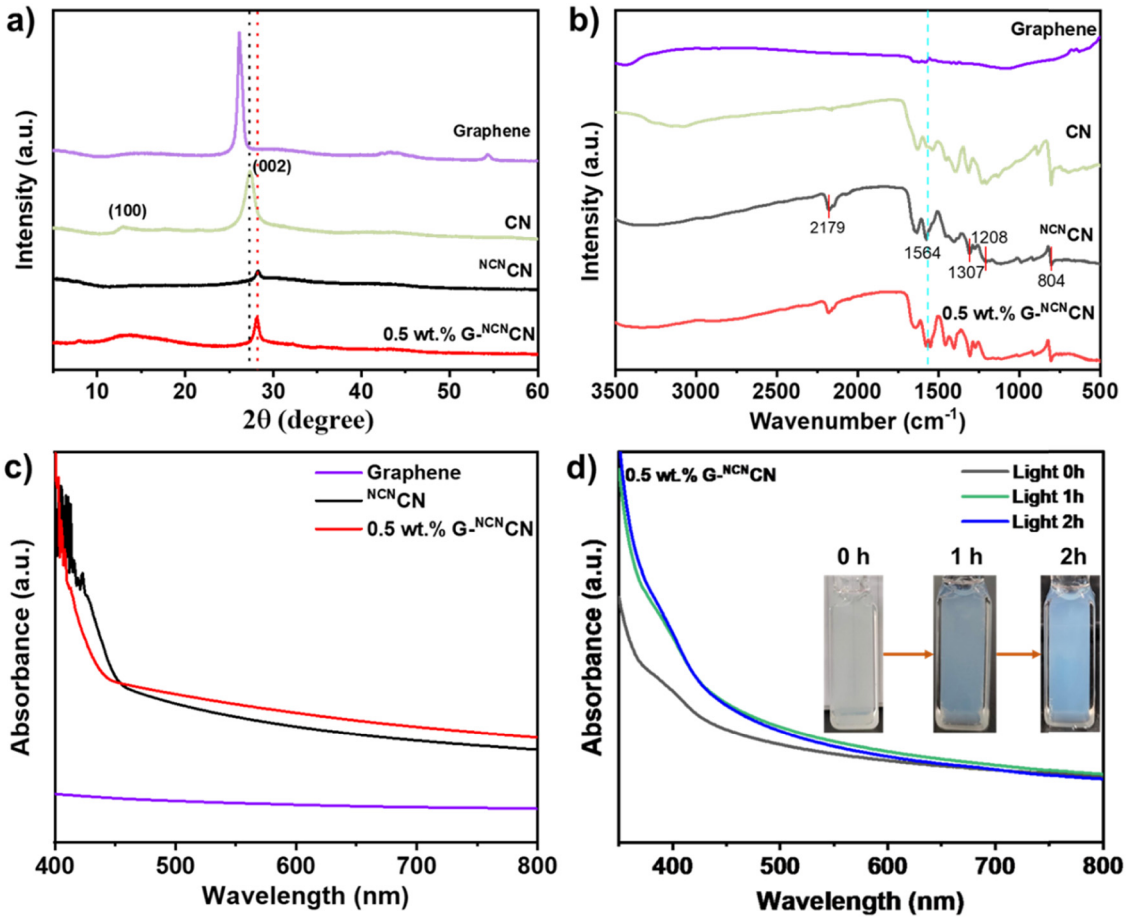

Fig. 1 (a) XRD patterns and (b) FT-IR spectra of CN, ^{NCN}CN, graphene, and 0.5 wt% G–^{NCN}CN. (c) UV-visible absorption spectra of ^{NCN}CN, graphene, and 0.5 wt% G–^{NCN}CN and (d) time-dependent UV-Vis absorption spectra of the 0.5 wt% G–^{NCN}CN sample.

absorption. Notably, the 0.5 wt% G–^{NCN}CN composite displays an intermediate absorption intensity that surpasses that of graphene and ^{NCN}CN alone. Therefore, the photocatalytic band structure diagram derived from Tauc plots and valence band maps is presented in Fig. S5. It can be observed that the band structure of the composite material has not undergone significant changes. However, compared to the individual components, the composite exhibits markedly enhanced absorption, suggesting a potential synergistic interaction between graphene and the ^{NCN}CN matrix. The improved light-harvesting efficiency serves as a key indicator of the composite's potential for enhanced photocatalytic performance. Fig. 1d shows the color changes in the photocatalytic system before illumination and after 1 h and 2 h of light exposure. A distinct shift from white to blue is observed, with the entire system appearing blue. This is because under light exposure, ^{NCN}CN transitions to an excited state, generating negatively charged radical anions accompanied by a color change.[31–33] The corresponding absorption changes are also evident in the UV-visible absorption spectrum. Similarly, the UV-visible absorption spectra of the pure ^{NCN}CN sample at different irradiation times are shown in Fig. S2, exhibiting a trend consistent with that of the 0.5 wt% G–^{NCN}CN sample.[25]

The morphology and microstructure of the G–^{NCN}CN composite were investigated using transmission electron microscopy (TEM). As shown in Fig. 2a and b, the ^{NCN}CN photocatalysts display the irregularly shaped particles with an average size of approximately 50 nm. The graphene exhibits a layered structure and tightly wraps around the ^{NCN}CN particle surfaces in the G–^{NCN}CN composites (Fig. 2c and d). Although no clear graphene lattice striations were captured, this may be attributed to graphene's low contrast and sensitivity to intense electron beams.[34] The interface between graphene and ^{NCN}CN is further revealed (Fig. 2e), and the edge of the lamellar graphene interface has carbon nitride with lattice fringes. The lattice fringes with a spacing of 1.1 nm are observed, which correspond to the (100) planes of carbon nitride. Moreover, in the post-reaction HRTEM image (Fig. S7), Pt particle lattice fringes are clearly observable, indicating that Pt particles have deposited on the catalyst surface. EDS analysis of the G–^{NCN}CN sample (Fig. S6) reveals that carbon (C) exhibits the most extensive distribution. Nitrogen (N) and potassium (K) are concentrated on the ^{NCN}CN sample surface, while some platinum (Pt) shows agglomeration. Overall, however, Pt remains uniformly distributed.

The pore structure and specific surface area of ^{NCN}CN and 0.5 wt% G–^{NCN}CN were analyzed using N_2 adsorption–desorption isotherms (Fig. 3a). Fig. 3a shows the mesoporous structure (2–50 nm) of the carbon catalyst, with 0.5 wt% G–^{NCN}CN exhibiting a higher pore volume (0.096 *vs.* 0.082 $cm^3\ g^{-1}$) and a larger specific surface area (61.88 *vs.* 52.53 $m^2\ g^{-1}$). The specific surface areas and pore volumes of ^{NCN}CN and 0.5 wt% G–^{NCN}CN are listed in Table S3.

X-ray photoelectron spectroscopy (XPS) was employed to elucidate the chemical composition and the chemical states of C, N, and K elements in the G–^{NCN}CN composite. The survey spectrum of Pt nanoparticles loaded with 0.5 wt% graphene (Fig. S3a) reveals the presence of C, N, and O, along with a distinct peak at 291 eV corresponding to K 2p, confirming the incorporation of potassium into the composite. Analysis of elemental content proportions also indicates the presence of K in both ^{NCN}CN and 0.5 wt% G–^{NCN}CN samples, along with increased C and O content upon graphene incorporation (Table S1). This indicates that the G–^{NCN}CN composite

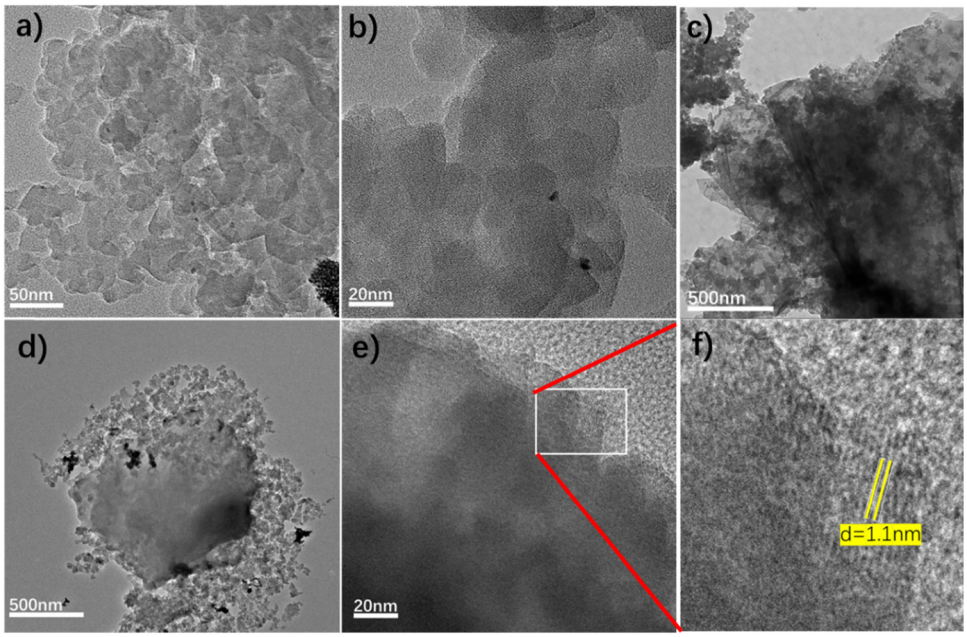

Fig. 2 (a) and (b) HRTEM images of pure ^{NCN}CN. (c) and (d) TEM images of the 0.5 wt% G–^{NCN}CN composites. (e) and (f) HRTEM images of the 0.5 wt% G–^{NCN}CN composites.

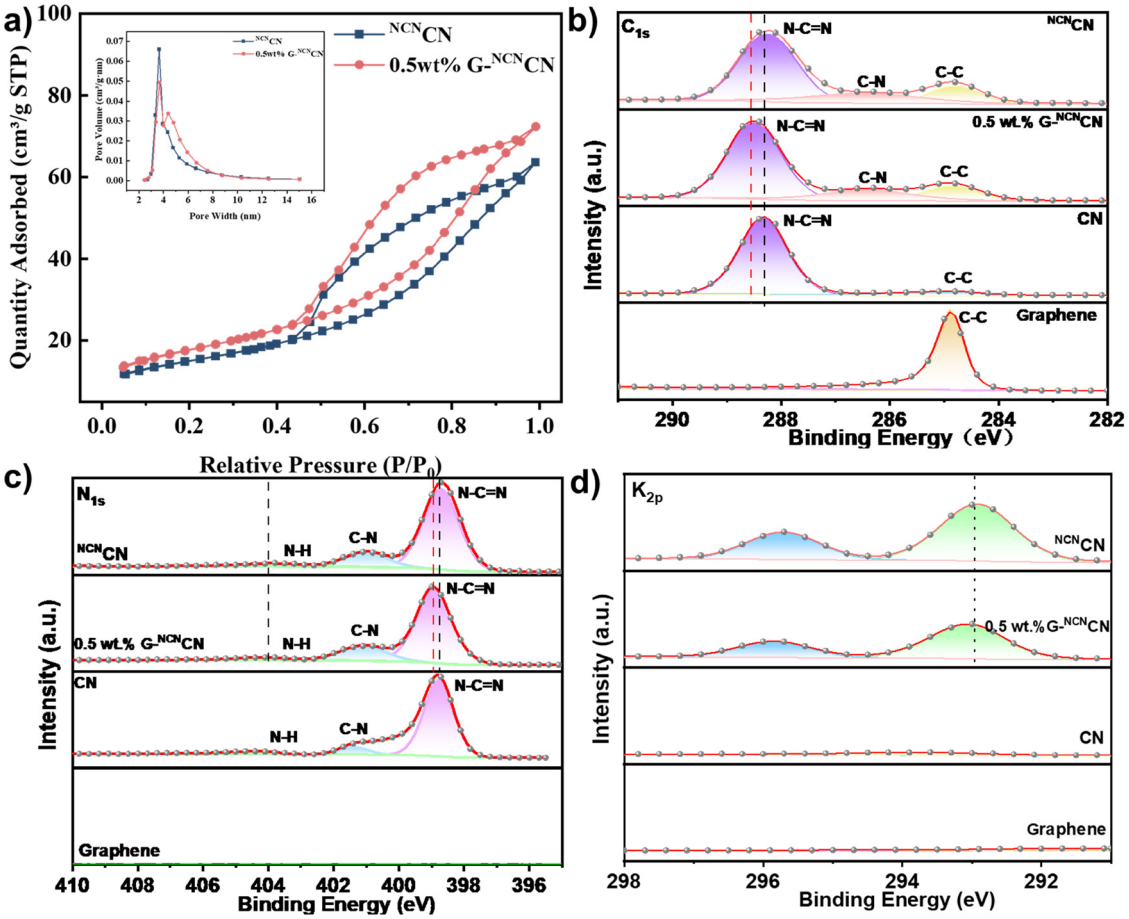

Fig. 3 (a) Nitrogen adsorption–desorption curve and pore size distribution curve of ^{NCN}CN and 0.5 wt% G–^{NCN}CN; (b) high-resolution C 1s XPS spectra of CN, ^{NCN}CN, graphene, and 0.5 wt% G–^{NCN}CN; (c) high-resolution N 1s XPS spectra of CN, ^{NCN}CN, graphene, and 0.5 wt% G–^{NCN}CN; and (d) high-resolution K 2p XPS spectra of CN, ^{NCN}CN, graphene, and 0.5 wt% G–^{NCN}CN.

photocatalyst is mainly composed of carbon, nitrogen, and oxygen and also contains potassium ions. In contrast, the XPS total spectrum of CN does not contain the K peak (Fig. S3b). As shown in Fig. 3b, the high-resolution C 1s spectra of ^{NCN}CN and 0.5 wt% G–^{NCN}CN can be deconvoluted into three primary components at binding energies of 284.8, 286.4, and 288.2 eV, corresponding to the C═C, C–N, and N–C═N bonds, respectively, which are characteristic of the heptazine rings in carbon nitride.[35] However, two additional peaks in the range of 292.9 and 295.7 eV in the ^{NCN}CN and 0.5 wt% G–^{NCN}CN (Fig. 3d) are assigned to K^+ ions, which are absent in pristine carbon nitride (CN). This is corroborated by the presence of anionic cyanamide groups in the distinct ^{NCN}CN structure observed in the preceding FT-IR spectrum, indicating that its charge is balanced by K^+ counterions.[26] As shown in Fig. 3c, the N 1s spectrum further corroborates the carbon nitride structure, displaying major peaks for sp^2-hybridized N in C–N═C (398.7 eV) and amino groups (C–NH_x, 401.0 eV), alongside a π-excitation peak at 404.4 eV. A notable observation is the consistent shift of these peaks to higher binding energies in the G–^{NCN}CN composite compared to its individual components. This positive shift suggests an enhanced π-electron delocalization across the heterojunction, likely induced by the electronic coupling between graphene and the CN matrix, which is beneficial for facilitating charge carrier separation.[26,36]

Time-resolved and steady-state photoluminescence spectroscopy (TRPL/PL) measurements conducted at room temperature (Fig. 4a and b) reveal significant differences between pristine ^{NCN}CN and 0.5 wt% G–^{NCN}CN. The steady-state PL spectra of ^{NCN}CN and G–^{NCN}CN, excited over a broad wavelength range, are shown in Fig. 4a. It can be observed that the PL spectrum of the G–^{NCN}CN sample is very similar to that of the pure ^{NCN}CN sample, with both samples exhibiting a main emission peak at around 470 nm (corrected from eV). However, compared to the pure ^{NCN}CN sample, the emission intensity of G–^{NCN}CN is reduced, indicating a higher separation rate of photogenerated electrons and holes in the composite under visible light irradiation. This can be attributed to graphene in the G–^{NCN}CN composite acting as a separation center for photogenerated electrons and holes. Under light irradiation, electrons in ^{NCN}CN are excited from the valence band to the conduction band and transfer to graphene. Due to its two-

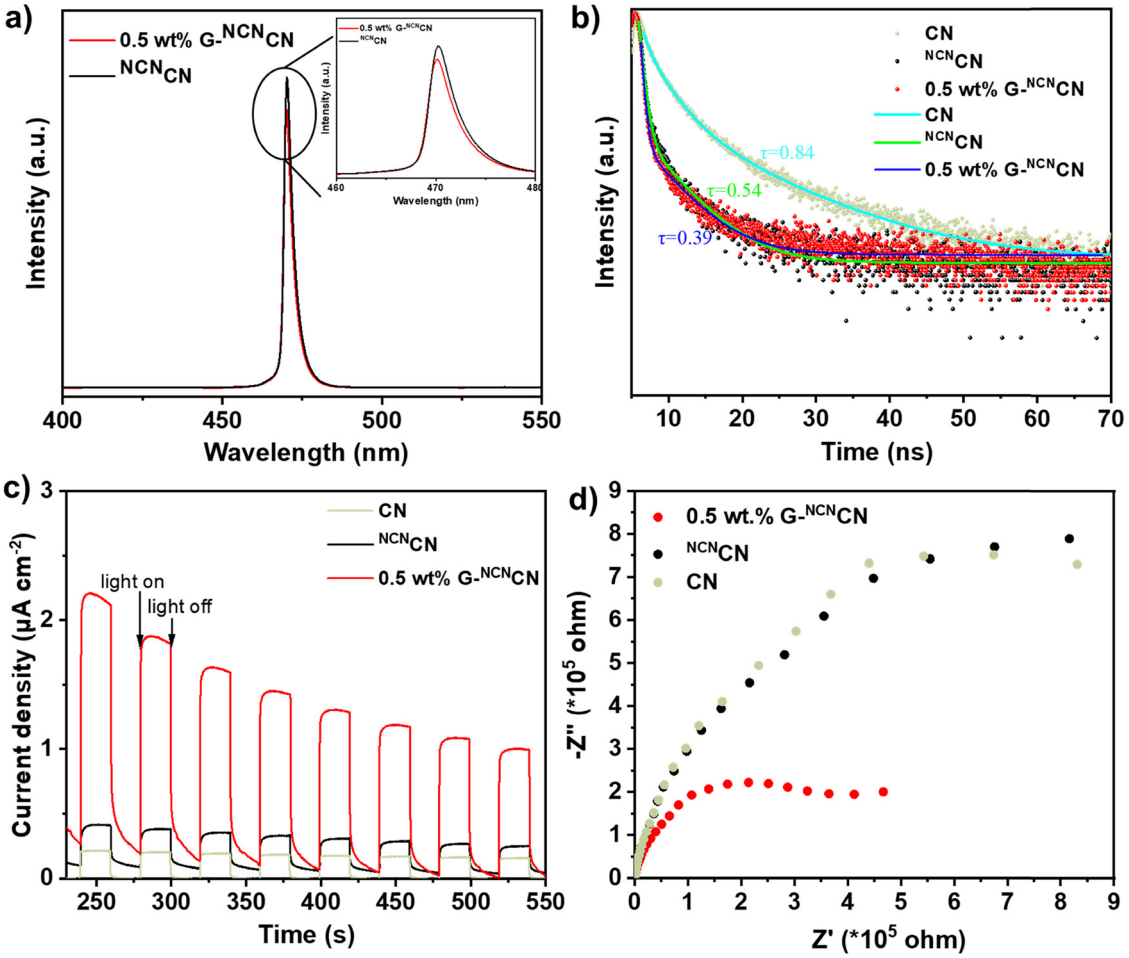

Fig. 4 (a) Photoluminescence spectra of the ^{NCN}CN and 0.5 wt% G–^{NCN}CN samples. (b) Time-resolved fluorescence spectroscopy spectra of CN, ^{NCN}CN and 0.5 wt% G–^{NCN}CN. (c) Transient photocurrent of CN, ^{NCN}CN and 0.5 wt% G–^{NCN}CN samples. (d) EIS Nyquist plots of CN, ^{NCN}CN and 0.5 wt% G–^{NCN}CN.

dimensional π-conjugated structure, graphene effectively prevents the recombination of photogenerated electrons and holes and is considered an excellent electron acceptor material.[20] Additionally, the measured fluorescence lifetime of 0.5 wt% G–^{NCN}CN is shorter than that of pure ^{NCN}CN and pure CN samples (Fig. 4b). This may be attributed to the bonding between graphene and the ^{NCN}CN matrix accelerating charge separation in ^{NCN}CN. Consequently, the shortened fluorescence lifetime may provide more opportunities for carriers to participate in the photocatalytic HER before recombination, thereby enhancing photocatalytic HER performance.

To further compare the charge separation and interfacial charge transfer efficiency of pure ^{NCN}CN and the G–^{NCN}CN composite sample, photocurrent tests were conducted on CN, ^{NCN}CN and 0.5 wt% G–^{NCN}CN samples using a standard three-electrode setup. As shown in Fig. 4c, it can be clearly seen that under illumination, the photocurrent intensity value increases rapidly, and when the light is turned off, the value decreases rapidly. Comparing the pure ^{NCN}CN sample, the G–^{NCN}CN composite sample shows higher photocurrent intensity. This significant enhancement in photocurrent intensity indicates that the G–^{NCN}CN composite sample has a lower recombination rate of photogenerated electron–hole pairs and stronger conductivity, which corroborates the PL spectroscopy conclusions and further proves that graphene promotes the separation efficiency of photogenerated charge carriers in the composite sample. In addition, electrochemical impedance spectroscopy (EIS) was performed on pure CN, pure ^{NCN}CN, and G–^{NCN}CN samples in a 0.2 M sodium sulfate solution. As shown in Fig. 4d, the resistance of the ^{NCN}CN sample is almost the same as that of the CN sample, with impedance of the ^{NCN}CN samples slightly lower than that of CN. In contrast, the G–^{NCN}CN sample shows a significant trend of reduced resistance. This indicates that the close interfacial contact between graphene and ^{NCN}CN can enhance photogenerated electron transfer and reduce the charge transfer barrier of ^{NCN}CN, thereby enhancing conductivity and photocatalytic activity.[37]

The photocatalytic performance of the material system was mainly evaluated through photocatalytic hydrogen production under light and the hydrogen production efficiency under dark conditions. Fig. 5a presents the photocatalytic hydrogen production performance of the G–^{NCN}CN samples with varying

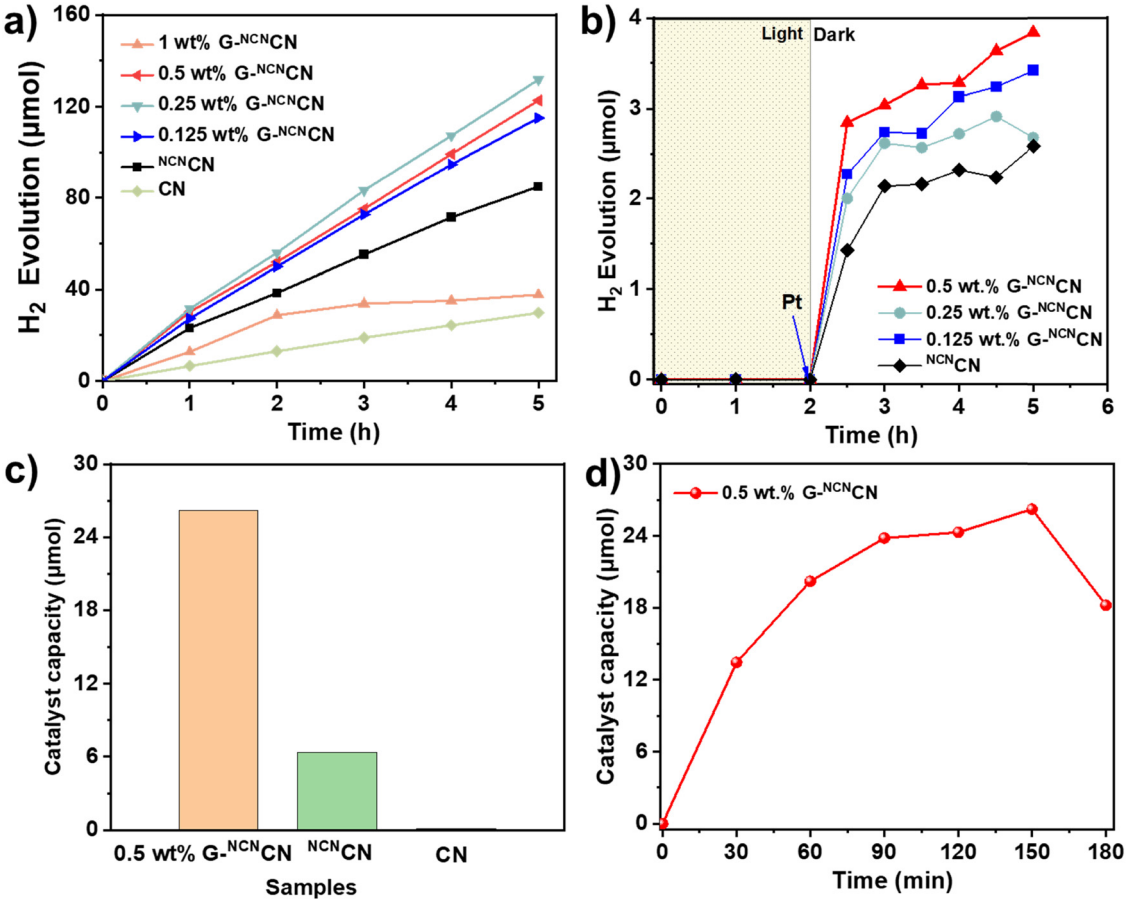

Fig. 5 (a) Photocatalytic hydrogen evolution performance of CN, ^{NCN}CN and the G–^{NCN}CN samples with the Pt cocatalyst. (b) Dark photocatalytic hydrogen production performance of the G–^{NCN}CN samples with different graphene amounts after adding the Pt cocatalyst. (c) Electron storage capacity of the CN, ^{NCN}CN and 0.5 wt% G–^{NCN}CN samples. (d) Time-dependent charge storage of the 0.5 wt% G–^{NCN}CN sample.

graphene weight ratios under continuous light irradiation. Compared to pure CN, pure ^{NCN}CN exhibits significantly enhanced activity, which can be attributed to its suitable band gap and distinctive electronic structure. After adding a small amount of graphene, the photocatalytic activity of the 0.125 wt% G–^{NCN}CN sample significantly increased. The hydrogen evolution rate increases with graphene content up to 0.25 wt%, reaching a maximum value of 3156 μmol h^{-1} g^{-1}. Meanwhile, Table S4 presents the hydrogen production performance of other carbon nitride/graphene-based composites. Apparent quantum efficiency (AQE) measurements at 450 nm yielded values of 0.21% for the ^{NCN}CN sample and 0.43% for the 0.5 wt% G–^{NCN}CN sample at the central wavelength of 450 nm (Table S2). However, further increasing the graphene content to 0.5 wt% and 1 wt% leads to a notable decline in photocatalytic activity. This reduction is likely due to increased opacity and light scattering, reducing radiation penetration through the reaction suspension. These results indicate that an appropriate graphene loading is crucial for optimizing the photocatalytic activity of the G–^{NCN}CN composite. Fig. 5b shows the hydrogen production yield plots for different samples discharging hydrogen in the dark after adding Pt nanoparticles following 2 hours of light irradiation. It can be seen that compared to the pure ^{NCN}CN sample, all mass ratios of G–^{NCN}CN materials showed increased yield after the addition of graphene, with the 0.5 wt% G–^{NCN}CN sample having the highest yield, reaching 3.8 μmol. This is likely because graphene promotes the separation of photogenerated electron–hole pairs in ^{NCN}CN, thereby increasing the electron storage capacity of the sample.[25]

To quantitatively determine the amounts of stored electrons in the G–^{NCN}CN composite system, methyl viologen (MV^{2+}) is utilized based on the principle that it undergoes a single-electron reduction process to form a distinctly blue radical cation (MV^{+}). By measuring the absorbance of the solution at 600 nm, the amount of MV^{+} generated during the quenching of G–^{NCN}CN by MV^{2+} was determined.[38] Therefore, the amount of MV^{+} equals the number of electrons accumulated in the catalyst.[33,39] As shown in Fig. 5c, using the above method, the electron storage capacity of the pure ^{NCN}CN sample was measured to be 6.3 μmol, whereas that of the 0.5 wt% G–^{NCN}CN composite sample reached 26.2 μmol, which is 4.2 times that of the pure ^{NCN}CN sample. Moreover, a noticeable difference in the intensity of the solution color was observed (as shown in Fig. S1). This phenomenon is likely attributed to the conductive network formed by graphene within the composite system, which enhances electron storage capacity. This conclusion is further supported by the subsequent hydrogen production

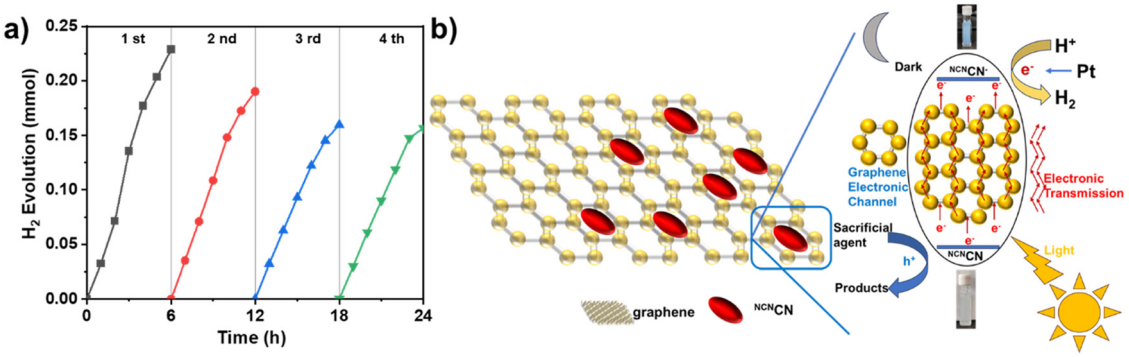

Fig. 6 (a) The recycling experiments of the 0.5 wt% G–^{NCN}CN photocatalyst. (b) Schematic of photocatalytic hydrogen production over the G–^{NCN}CN sample under light and dark conditions.

experiments conducted in dark environments. The effect of different illumination durations on stored photoelectrons is shown in Fig. 5d. It is evident that as the illumination time increases, the stored electron quantity continues to rise until the sacrificial agent is completely depleted.

The stability of the 0.5 wt% G–^{NCN}CN composite was evaluated through cyclic experiments under identical photocatalytic conditions (Fig. 6a). Over four consecutive cycles, hydrogen production decreased in the last three cycles compared to the first cycle, However, Fig. S8 shows the XRD comparison of the G–^{NCN}CN sample before and after the reaction. It can be observed that the XRD patterns of the sample remain virtually unchanged before and after the reaction. This indicates that the structure of the G–^{NCN}CN sample has not undergone significant alteration. Fig. S9 presents an image of the G–^{NCN}CN sample after centrifugation at 10 000 rpm for 5 minutes. This indicates that the sample exhibits excellent dispersibility in solution, potentially leading to losses during centrifugation, washing, and supernatant decantation. This may explain the slight decrease in hydrogen yield observed during the cycling test. Nevertheless, the G–^{NCN}CN sample retained 80% of its initial hydrogen production capacity after four cycles, demonstrating considerable stability. Naturally, such losses are undesirable, and future plans will focus on addressing this issue.

The mechanism underlying the high hydrogen evolution activity of the sample under visible light irradiation can be explained as shown in Fig. 6b. Under visible light irradiation, electrons (e^-) transition from the valence band (VB) formed by the N 2p orbitals to the conduction band (CB) formed by the C 2p orbitals in the ^{NCN}CN molecule, thereby generating holes (h^+) in the valence band. Typically, these carriers rapidly recombine, and due to Schottky barrier limitations, only a fraction of electrons are injected into Pt nanoparticles.[40] The injected electrons accumulate on the Pt nanoparticle surface, effectively reducing H_2O (or H^+) to produce H_2. Meanwhile, the holes accumulate in the VB of ^{NCN}CN and react with triethanolamine, which acts as a sacrificial agent. When ^{NCN}CN is immobilized on graphene sheets to form a layered composite, the excellent conductivity of graphene facilitates the transfer of these photo-generated electrons to the graphene sheets, enhancing hole–electron separation. The transferred electrons accumulate at the Pt nanoparticles loaded on the graphene sheets *via* the electronic pathways of graphene, subsequently participating in H_2 generation. Without loaded platinum nanoparticles, the photo-generated electrons produced by ^{NCN}CN transfer to graphene, achieving electron–hole separation. Excess holes react with 4-MBA as a sacrificial agent, while electrons are absorbed and stored within the ^{NCN}CN structure *via* the cyanide-potassium ion pair through the graphene electron channel. When illumination ceases and the environment darkens, the photogenerated electrons remain stored until platinum nanoparticles intervene, at which point the stored electrons are transferred to participate in the H_2 generation reaction.

4. Conclusions

In summary, a G–^{NCN}CN composite was prepared in this study *via* physical mixing and the effect of graphene loading on the structure and performance of the G–^{NCN}CN composite photocatalyst was investigated. After introducing graphene, ^{NCN}CN was immobilized on the graphene surface to form a layered composite. Graphene acts as a conductive channel, effectively separating photogenerated charge carriers, improving the visible-light photocatalytic hydrogen production activity, and simultaneously increasing its electron storage capacity in dark environments. The results show that the optimal graphene content is 0.5 wt%, with a corresponding hydrogen production rate of 3156 μmol h^{-1} g^{-1}, which is approximately 35% higher than that of the pure ^{NCN}CN sample. Furthermore, the hydrogen production amount in the dark reached 3.8 μmol, about 65% higher than that of the pure ^{NCN}CN sample. Photoluminescence and photocurrent response data further confirmed that graphene can act as a good acceptor for photogenerated electrons, thereby hindering the recombination of electron–hole pairs. This work demonstrates that G–^{NCN}CN is a highly promising candidate composite material, potentially useful for developing high-performance photocatalysts and inexpensive metal-free G–^{NCN}CN composites with high visible-light photocatalytic activity.

Author contributions

Zejun Zhang: data curation, formal analysis, writing – original draft, and writing – review and editing. Fankai Bu: formal analysis and writing – review and editing. Zhidong Wei: formal analysis and writing – review and editing. Songmei Wang: formal analysis and writing – review and editing. Yong Zhu: supervision, data curation, formal analysis, and writing – review and editing. Junying Liu: conceptualization, funding acquisition, supervision, formal analysis, methodology, and writing – review and editing.

Conflicts of interest

There are no conflicts to declare.

Data availability

All relevant data are included in the paper or its supplementary information (SI). Supplementary information is available. See DOI: https://doi.org/10.1039/d6ya00031b.

Acknowledgements

This work was supported by the Jiangsu Distinguished Professor Project (RC20240909) and the Jiangsu University Foundation (no. 22JDG033).

References

1 C. F. Shih, T. Zhang, J. Li and C. Bai, Powering the Future with Liquid Sunshine, *Joule*, 2018, **2**, 1925–1949.
2 A. Fujishima and K. Honda, Electrochemical Photolysis of Water at a Semiconductor Electrode, *Nature*, 1972, **238**, 37–38.
3 S. Chen, T. Takata and K. Domen, Particulate photocatalysts for overall water splitting, *Nat. Rev. Mater.*, 2017, **2**, 17050.
4 Y. Tang, W. Zhou, Q. Shang, Y. Guo, H. Hu, Z. Li, Y. Zhang, L. Liu, H. Wang, X. Tan, T. Yu and J. Ye, Discerning the mechanism of expedited interfacial electron transformation boosting photocatalytic hydrogen evolution by metallic 1T-WS2-induced photothermal effect, *Appl. Catal., B*, 2022, **310**, 121295.
5 S. Wang, J. Zhang, B. Li, H. Sun and S. Wang, Engineered Graphitic Carbon Nitride-Based Photocatalysts for Visible-Light-Driven Water Splitting: A Review, *Energy Fuels*, 2021, **35**, 6504–6526.
6 N. Ishak, V. Jeyalakshmi, M. Setka, M. Grandcolas, B. Devadas and M. Šoóš, Upgrading of g-C3N4 semiconductor by a Nitrogen-doped carbon material: A photocatalytic degradation application, *J. Environ. Chem. Eng.*, 2023, **11**, 109381.
7 G. Liu, H. Lv, Y. Zeng, M. Yuan, Q. Meng, Y. Wang and C. Wang, Single-Atom Pd–N3 Sites on Carbon-Deficient g-C3N4 for Photocatalytic H2 Evolution, *Trans. Tianjin Univ.*, 2021, **27**, 139–146.
8 S. C. Yan, Z. S. Li and Z. G. Zou, Photodegradation Performance of g-C3N4 Fabricated by Directly Heating Melamine, *Langmuir*, 2009, **25**, 10397–10401.
9 Y. Zheng, J. Liu, J. Liang, M. Jaroniec and S. Z. Qiao, Graphitic carbon nitride materials: controllable synthesis and applications in fuel cells and photocatalysis, *Energy Environ. Sci.*, 2012, **5**, 6717–6731.
10 J. Qin, S. Wang, H. Ren, Y. Hou and X. Wang, Photocatalytic reduction of CO2 by graphitic carbon nitride polymers derived from urea and barbituric acid, *Appl. Catal., B*, 2015, **179**, 1–8.
11 M. F. Vega, C. Olivas, E. Díaz-Faes and C. Barriocanal, Evaluation of water splitting efficiency of g-C3N4 thermally etched/exfoliated under air and CO2 atmospheres, *Catal. Today*, 2024, **427**, 114412.
12 J. Qin, Y. Jiao, M. Liu, Y. Li and J. Wang, Heat treatment to prepare boron doped g-C3N4 nanodots/carbon-rich g-C3N4 nanosheets heterojunction with enhanced photocatalytic performance for water splitting hydrogen evolution, *J. Alloys Compd.*, 2022, **898**, 162846.
13 Y. Zhang, T. Mori, J. Ye and M. Antonietti, Phosphorus-Doped Carbon Nitride Solid: Enhanced Electrical Conductivity and Photocurrent Generation, *J. Am. Chem. Soc.*, 2010, **132**, 6294–6295.
14 G. Liu, P. Niu, C. Sun, S. C. Smith, Z. Chen, G. Q. Lu and H.-M. Cheng, Unique Electronic Structure Induced High Photoreactivity of Sulfur-Doped Graphitic C3N4, *J. Am. Chem. Soc.*, 2010, **132**, 11642–11648.
15 P. Sharma, P. P. Sarngan, A. Lakshmanan and D. Sarkar, One-step synthesis of highly reactive g-C3N4, *J. Mater. Sci.: Mater. Electron.*, 2022, **33**, 9116–9125.
16 K. Sridharan, E. Jang and T. J. Park, Novel visible light active graphitic C3N4–TiO2 composite photocatalyst: Synergistic synthesis, growth and photocatalytic treatment of hazardous pollutants, *Appl. Catal., B*, 2013, **142–143**, 718–728.
17 Y. Hong, Y. Jiang, C. Li, W. Fan, X. Yan, M. Yan and W. Shi, In-situ synthesis of direct solid-state Z-scheme V2O5/g-C3N4 heterojunctions with enhanced visible light efficiency in photocatalytic degradation of pollutants, *Appl. Catal., B*, 2016, **180**, 663–673.
18 D. Zheng, G. Zhang and X. Wang, Integrating CdS quantum dots on hollow graphitic carbon nitride nanospheres for hydrogen evolution photocatalysis, *Appl. Catal., B*, 2015, **179**, 479–488.
19 A. Geim and K. Novoselov, Graphene calling, *Nat. Mater.*, 2007, **6**, 169.
20 A. K. Geim, Graphene: Status and Prospects, *Science*, 2009, **324**, 1530–1534.
21 H. Zhang, X. Lv, Y. Li, Y. Wang and J. Li, P25-Graphene Composite as a High Performance Photocatalyst, *ACS Nano*, 2010, **4**, 380–386.
22 Q. Xiang, J. Yu and M. Jaroniec, Preparation and Enhanced Visible-Light Photocatalytic H2-Production Activity of Graphene/C3N4 Composites, *J. Phys. Chem. C*, 2011, **115**, 7355–7363.
23 J. Liu, H. Xu, Y. Xu, Y. Song, J. Lian, Y. Zhao, L. Wang, L. Huang, H. Ji and H. Li, Graphene quantum dots modified

mesoporous graphite carbon nitride with significant enhancement of photocatalytic activity, *Appl. Catal., B*, 2017, **207**, 429–437.

24 M. Sakar, C.-C. Nguyen, M.-H. Vu and T.-O. Do, Materials and Mechanisms of Photo-Assisted Chemical Reactions under Light and Dark Conditions: Can Day–Night Photocatalysis Be Achieved?, *ChemSusChem*, 2018, **11**, 809–820.

25 V. W.-h Lau, D. Klose, H. Kasap, F. Podjaski, M.-C. Pignié, E. Reisner, G. Jeschke and B. V. Lotsch, Dark Photocatalysis: Storage of Solar Energy in Carbon Nitride for Time-Delayed Hydrogen Generation, *Angew. Chem., Int. Ed.*, 2017, **56**, 510–514.

26 D. Gunawan, C. Y. Toe, P. Kumar, J. Scott and R. Amal, Synergistic Cyanamide Functionalization and Charge-Induced Activation of Nickel/Carbon Nitride for Enhanced Selective Photoreforming of Ethanol, *ACS Appl. Mater. Interfaces*, 2021, **13**, 49916–49926.

27 G. Wang, J. Yang, J. Park, X. Gou, B. Wang, H. Liu and J. Yao, Facile Synthesis and Characterization of Graphene Nanosheets, *J. Phys. Chem. C*, 2008, **112**, 8192–8195.

28 V. W.-h Lau, I. Moudrakovski, T. Botari, S. Weinberger, M. B. Mesch, V. Duppel, J. Senker, V. Blum and B. V. Lotsch, Rational design of carbon nitride photocatalysts by identification of cyanamide defects as catalytically relevant sites, *Nat. Commun.*, 2016, **7**, 12165.

29 E. Horvath-Bordon, E. Kroke, I. Svoboda, H. Fuess and R. Riedel, Potassium melonate, K3[C6N7(NCN)3]·5H2O, and its potential use for the synthesis of graphite-like C3N4 materials, *New J. Chem.*, 2005, **29**, 693–699.

30 C. Nethravathi and M. Rajamathi, Chemically modified graphene sheets produced by the solvothermal reduction of colloidal dispersions of graphite oxide, *Carbon*, 2008, **46**, 1994–1998.

31 H. Ou, C. Tang, X. Chen, M. Zhou and X. Wang, Solvated Electrons for Photochemistry Syntheses Using Conjugated Carbon Nitride Polymers, *ACS Catal.*, 2019, **9**, 2949–2955.

32 B. Kurpil, Y. Markushyna and A. Savateev, Visible-Light-Driven Reductive (Cyclo)Dimerization of Chalcones over Heterogeneous Carbon Nitride Photocatalyst, *ACS Catal.*, 2019, **9**, 1531–1538.

33 A. Savateev, B. Kurpil, A. Mishchenko, G. Zhang and M. Antonietti, A ''waiting'' carbon nitride radical anion: a charge storage material and key intermediate in direct C–H thiolation of methylarenes using elemental sulfur as the ''S''-source, *Chem. Sci.*, 2018, **9**, 3584–3591.

34 P. Plachinda, S. Rouvimov and R. Solanki, Structure analysis of CVD graphene films based on HRTEM contrast simulations, *Phys. Status Solidi A*, 2011, **208**, 2681–2687.

35 T. Uekert, H. Kasap and E. Reisner, Photoreforming of Nonrecyclable Plastic Waste over a Carbon Nitride/Nickel Phosphide Catalyst, *J. Am. Chem. Soc.*, 2019, **141**, 15201–15210.

36 N. Liu, T. Li, Z. Zhao, J. Liu, X. Luo, X. Yuan, K. Luo, J. He, D. Yu and Y. Zhao, From Triazine to Heptazine: Origin of Graphitic Carbon Nitride as a Photocatalyst, *ACS Omega*, 2020, **5**, 12557–12567.

37 P. Tiong, H. O. Lintang, S. Endud and L. Yuliati, Improved interfacial charge transfer and visible light activity of reduced graphene oxide–graphitic carbon nitride photocatalysts, *RSC Adv.*, 2015, **5**, 94029–94039.

38 T. Watanabe and K. Honda, Measurement of the extinction coefficient of the methyl viologen cation radical and the efficiency of its formation by semiconductor photocatalysis, *J. Phys. Chem.*, 1982, **86**, 2617–2619.

39 Y. Markushyna, P. Lamagni, C. Teutloff, J. Catalano, N. Lock, G. Zhang, M. Antonietti and A. Savateev, Green radicals of potassium poly(heptazine imide) using light and benzylamine, *J. Mater. Chem. A*, 2019, **7**, 24771–24775.

40 J. Yu, L. Qi and M. Jaroniec, Hydrogen Production by Photocatalytic Water Splitting over Pt/TiO2 Nanosheets with Exposed (001) Facets, *J. Phys. Chem. C*, 2010, **114**, 13118–13125.